

# Superconductivity and Shubnikov–de Haas oscillations in the noncentrosymmetric half-Heusler compound YPtBi

Orest Pavlosiuk, Dariusz Kaczorowski, and Piotr Wiśniewski

*Institute of Low Temperature and Structure Research, Polish Academy of Sciences, P. O. Box 1410, 50-950 Wrocław, Poland*

(Received 4 February 2016; revised manuscript received 8 June 2016; published 13 July 2016)

Recent findings of possible topological superconductivity in YPtBi motivated us to grow and investigate single crystals of this material. The compound was studied by means of ac magnetic susceptibility, electrical resistivity, Hall resistivity, and heat capacity measurements, performed in wide ranges of temperature and magnetic field. The superconductivity below the critical temperature  $T_c = 0.97$  K was clearly reflected in the magnetic and electronic transport data. The upper critical field  $B_{c2}$  was estimated at 1.84 T. However, no obvious anomaly near  $T_c$  was found in the temperature dependence of the heat capacity. In the normal state YPtBi appears semimetallic but its electrical conductance can be described by two components corresponding to parallel channels: metallic and semiconducting, with the latter becoming negligible at temperatures below 40 K. Shubnikov–de Haas oscillations were observed at temperatures below 10 K. Nontrivial Berry phase together with weak antilocalization effect strongly support the presence of Dirac fermions in YPtBi.

DOI: [10.1103/PhysRevB.94.035130](https://doi.org/10.1103/PhysRevB.94.035130)

## I. INTRODUCTION

The ternary bismuthide YPtBi belongs to the outstanding class of intermetallic materials, crystallizing in MgAgAs-type structure, known as half-Heusler phases [1]. Since the late 1990s half-Heusler compounds gained profound interest as new multifunctional materials for spintronic and thermoelectric applications [2]. In the course of time, new properties and putative fields of applications appeared continuously. Recent discoveries of topological properties revive the interest in the half-Heusler phases containing heavy elements. Several research groups have independently predicted theoretically a 3D topological insulator state (TI) in some of these compounds [3–6]. Furthermore, some representatives of half-Heusler family are low-temperature superconductors, YPtBi among them [7–15]. Due to its noncentrosymmetric crystal structure YPtBi might be an unconventional superconductor with mixed spin-singlet/spin-triplet pairing. Based on the results of first principles calculations of the electron-phonon coupling in YPtBi, it has recently been concluded that the mechanism of pairing in YPtBi is indeed unconventional [16]. Besides, combination of nontrivial 3D topology and superconductivity makes YPtBi one of the leading candidates for realizing topological superconducting state.

TIs have gapless conducting surface states protected from backscattering by time-reversal symmetry. Nevertheless, surface states of a superconducting TI may host Majorana fermions [17], which spark considerable interest because of their potential application in building a fault-tolerant quantum computer [18]. Immediately after discovery of superconductivity in copper doped  $\text{Bi}_2\text{Se}_3$  [19], Fu and Berg theoretically predicted that  $\text{Cu}_x\text{Bi}_2\text{Se}_3$  could be a topological superconductor (TSC) [20]. The observation of topological order together with superconductivity in that compound [21] has given a powerful impetus to the intensive development in the field of TSCs. In addition to  $\text{Cu}_x\text{Bi}_2\text{Se}_3$  and a group of a half-Heusler phases, several other compounds were proposed as putative TSCs, usually doped topological crystalline insulators [22,23] or doped-TI heterostructures [24,25].

YPtBi has hitherto been investigated thoroughly in view of the superconductivity, occurring below critical temperature,  $T_c = 0.77$  K [7–9], whereas a possible topological nontriviality of its electronic state was studied to a much lesser degree [7,26]. Therefore, the main goal of the present work was to gather evidence in support of nontrivial topology of the electronic structure in YPtBi. There are several experimental methods for verification of topological nontriviality, with the most straightforward being surface-sensitive probes, such as angle-resolved photoemission spectroscopy and scanning tunneling spectroscopy, which in the case of half-Heusler phases are hampered by strong difficulties with preparation of clean surface [27]. Recently, nuclear magnetic resonance has been suggested to be a simple technique probing band inversion in half-Heusler bismuthides, among them YPtBi, a necessary condition for realizing nontrivial topology [26,28]. In this paper, we focused our attention on the magnetotransport properties of single-crystalline YPtBi, expected to provide further fingerprints of its nontrivial topological nature [29].

## II. EXPERIMENTAL DETAILS

Single crystals of YPtBi were grown from Bi flux with the starting atomic composition Y:Pt:Bi of 1:1:9. First, binary equiatomic compound YBi was prepared by arc melting. Then, it was crushed, mixed with small pieces of Pt wires and Bi grains, put in an alumina crucible, and sealed in an evacuated quartz ampule. The ampule was heated slowly to 1130 °C and kept for 12 h, then slowly cooled down to 925 °C at 3 °C/h and kept for 12 h. Afterwards, the cooling continued at 1 °C/h rate down to 550 °C, and at that temperature the ampule was taken out from the furnace. The excess of Bi flux was removed by etching with diluted nitric acid. The obtained single crystals had shapes of truncated pyramids with the dimensions up to  $1.5 \times 1.5 \times 1.8$  mm<sup>3</sup>.

Several single crystals were powdered and x-ray diffraction at room temperature was used to verify the  $F\bar{4}3m$  space group and to determine the lattice parameter of 6.65 Å,

using an X'pert Pro PANalytical diffractometer with Cu- $K\alpha$  radiation.

Chemical composition of the obtained YPtBi single crystals was studied on a FEI scanning electron microscope equipped with an EDAX Genesis XM4 spectrometer. The crystals were found homogeneous with Y:Pt:Bi ratio of 28.3:38:33.7, within experimental error of  $\pm 3\%$ , indistinguishable from 34.6:32.5:32.9 of Ref. [30].

ac magnetic susceptibility measurements were performed on a collection of small YPtBi single crystals with the total mass of 167 mg. These experiments were carried out in the temperature interval 0.45–2.0 K using a Quantum Design MPMS-XL SQUID magnetometer with an iHelium3 refrigerator.

For electrical transport studies, specimens of bar and platelet shapes were cut from two single crystals and then polished. Dimensions of samples were  $0.20 \times 0.29 \times 1.2 \text{ mm}^3$  for resistivity measurements and  $0.15 \times 0.44 \times 1.6 \text{ mm}^3$  for Hall resistivity measurements. Standard ac four-probe method was used for these two experiments with electrical leads made of 50- $\mu\text{m}$ -diameter silver wire spot-welded to the samples and additionally fixed with silver paste. The experiments were conducted in the temperature range 0.4–300 K and in applied magnetic fields up to 9 T using a Quantum Design PPMS platform with a  $^3\text{He}$  refrigerator. In magnetoresistance measurements electric current was flowing along  $[1\ 0\ 0]$  and the field applied in  $[0\ 0\ 1]$  crystallographic direction, whereas in the Hall resistivity measurements the current direction was  $[1\ \bar{1}\ 0]$  and the field direction was  $[1\ 1\ 1]$ .

Heat capacity measurements were carried out within the temperature range 0.4–20 K on a 46.5 mg collection of YPtBi single crystals using a relaxation method implemented into the PPMS platform.

### III. RESULTS AND DISCUSSION

#### A. Magnetic susceptibility

Low-temperature dependencies of the real,  $\chi'_{ac}$ , and imaginary,  $\chi''_{ac}$ , components of the ac magnetic susceptibility of YPtBi are depicted in Fig. 1(a). Abrupt drop of  $\chi'_{ac}$  clearly indicates a superconducting phase transition at  $T_c = 0.86 \text{ K}$ , which agrees with the values reported in the literature [7–9]. The  $\chi'_{ac}$  component does not saturate down to the lowest available temperature of 0.45 K, at which only the 54% magnetic screening factor is achieved. Similar lack of saturation of the magnetic susceptibility of YPtBi in the superconducting state was also noticed by Butch *et al.* [7] and Bay *et al.* [9]. This behavior confirms very small magnitude of the lower critical field in this material ( $\approx 5 \mu\text{T}$  at 0.5 K in Ref. [9]).

#### B. Electrical transport

Figure 1(b) represents the temperature variation of the electrical resistivity of single-crystalline YPtBi. The shape of  $\rho(T)$  reflects a semiconducting character of our sample. On cooling below 300 K, the resistivity gradually increases, indicating the presence of a band gap, and levels off below 70 K. The value of  $\rho$  at 300 K is 0.52 m $\Omega \text{ cm}$ , and at 2 K it is 0.88 m $\Omega \text{ cm}$ . In general, as regards both the magnitude of

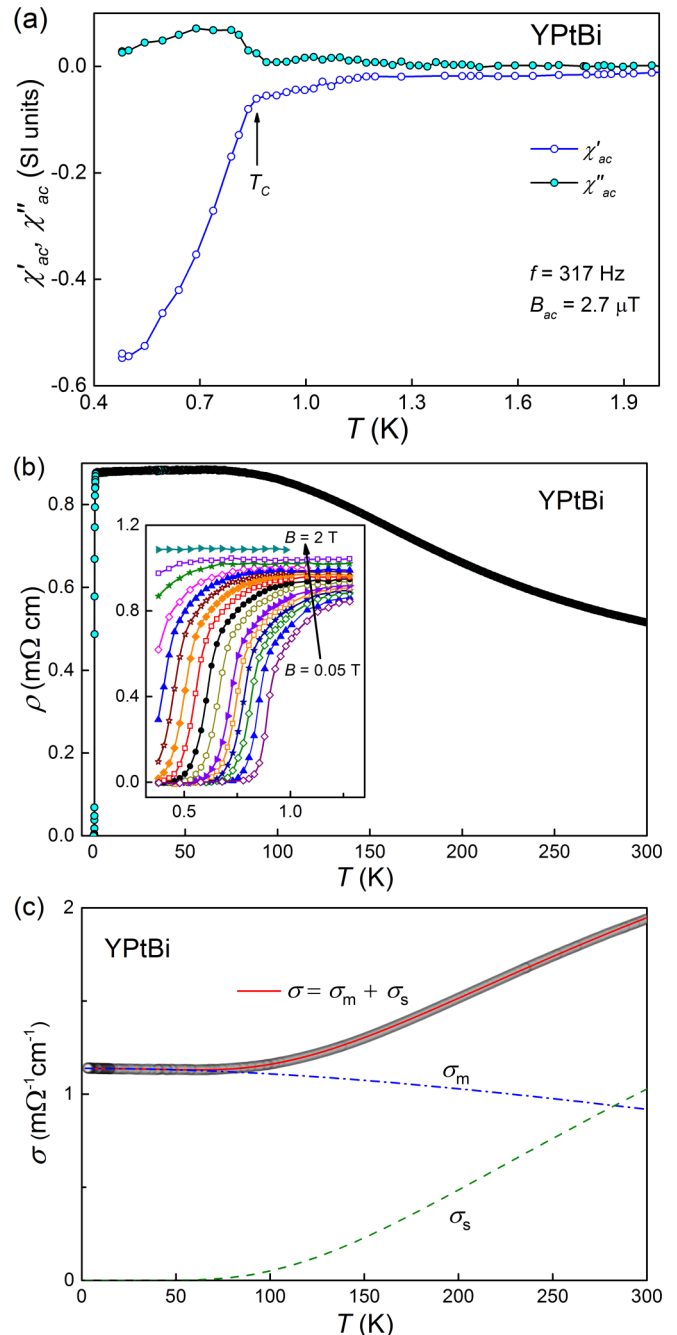


FIG. 1. (a) Temperature variations of the real (empty circles) and imaginary (filled circles) components of the ac magnetic susceptibility of YPtBi. The arrow marks the critical temperature. (b) Temperature dependence of the electrical resistivity of YPtBi in zero magnetic field. Inset: blowup of low-temperature resistivity revealing the superconducting transition, measured in different applied magnetic fields from 0.05 to 2 T range. (c) Temperature variation of the electrical conductivity of YPtBi in the normal state. The red solid line represents the fitting with two-channel charge transport model; dashed (green) and dash-dotted (blue) lines correspond to the semiconducting and metallic channels, respectively.

the resistivity and its temperature variation, our single crystals resemble those studied by Butch *et al.* [7]. In contrast, Bay *et al.* observed a metallic behavior of their single crystals in the

entire temperature range covered [8], while the polycrystalline samples investigated by Shekhar *et al.* showed  $\rho(T)$  with well pronounced broad maximum near 120 K [30].

A sharp drop in the resistivity at low temperatures signals the onset of the superconducting state. The critical temperature, defined as a point in which resistivity drops to 50% of its value at the onset of its bending down, amounts to 0.97 K. The resistivity drops to zero below 0.85 K, indicating the formation of continuous superconducting current paths, in good agreement with literature data [7,9]. However, the width of the superconducting transition  $\Delta T_c = 0.45$  K is consistent with the broad anomaly observed in the temperature-dependent ac magnetic susceptibility, but even larger than 0.36 K of Ref. [9]. Those authors found the midpoint of the transition at 0.98 K, nearly identical with our value of  $T_c$ . Other studies showed much narrower transitions with  $T_c \approx 0.8$  K [7,8,30]. This may point to some superconducting impurities or inhomogeneities widening the transition in our sample, but undetectable by sample-quality characterization techniques we have at our disposal.

The low-temperature resistivity of YPtBi, measured in various external magnetic fields up to 2 T, is shown in the inset to Fig. 1(b). With increasing the field strength, the superconducting transition shifts to lower temperatures. The value of upper critical field,  $B_{c2} = 0.9$  T, at our lowest temperature of 0.4 K is slightly larger than 0.75 T presented in Ref. [7]. Rough extrapolation of our data to  $T = 0$  yielded  $B_{c2}(0) \approx 1.6$  T.

The superconducting coherence length,  $\xi_0$ , in YPtBi can be calculated from the formula  $\xi_0 = \sqrt{\Phi_0/2\pi B_{c2}(0)}$ , where  $\Phi_0$  is the flux quantum. The so-obtained value  $\xi_0 = 14$  nm is very similar to those reported in Refs. [7,8]. Under assumption that Fermi surface (FS) is spherical, the Fermi wave number,  $k_F$ , can be determined as  $k_F = (3\pi^2 n)^{1/3}$ , where  $n$  is the carrier concentration. Setting  $n = n_H = 5.6 \times 10^{18} \text{ cm}^{-3}$  from the Hall effect data (see below) one obtains  $k_F = 5.5 \times 10^6 \text{ cm}^{-1}$ . Then, with the residual resistivity  $\rho_0 = 0.88 \text{ m}\Omega \text{ cm}$ , one finds the mean free path  $l = \hbar k_F / \rho_0 n e^2 = 67 \text{ nm}$ . The latter value is significantly larger than  $\xi_0$ , which provides further proof that the superconductivity in YPtBi occurs in the clean limit. Pauli limiting field,  $B_P$ , can be calculated from the expression  $B_P = \Delta / \sqrt{2} \mu_B$ , where  $\Delta = 1.76 k_B T_c$  is the BCS energy gap. The so-derived  $B_P = 1.8$  T is close to  $B_{c2}$ , which implies that the superconductivity in YPtBi is Pauli limited.

As shown in Fig. 1(c), the overall behavior of the electrical conductivity,  $\sigma(T)$ , of YPtBi can be well approximated by the two-channel charge transport model, recently applied to describe the  $\sigma(T)$  dependence in LuPdBi [14]. The conductivity is assumed to be a sum of contributions from two independent channels: metallic- and semiconductinglike. For the metallic channel it is described by  $\sigma_m(T) = 1/(\rho_0 + bT^2)$ , where  $\rho_0$  is the residual resistivity due to scattering on structural defects, while the second term represents electron-electron scattering processes. In turn, the semiconducting channel contributes with  $\sigma_s(T) = 1/(a \exp(-E_g/k_B T))$ , where  $E_g$  is an energy gap between valence and conduction bands. Fitting  $\sigma(T) = \sigma_m(T) + \sigma_s(T)$  to the experimental data of YPtBi, in the temperature range 2–300 K, yielded the following parameters:  $a = 217 \text{ m}\Omega \text{ cm}$ ,  $E_g = 38.8 \text{ meV}$ , and  $b = 2.3 \text{ n}\Omega \text{ cm/K}^2$ . The  $E_g$  value is about four times larger than 11.5 meV found

for LuPdBi in Ref. [14], thus indicating that YPtBi is more “bulk-insulating” material than LuPdBi. Furthermore, it is worth noting that below 40 K, conductivity of the semiconductinglike channel becomes negligible and the electric current essentially flows through the metalliclike channel. For LuPdBi the analogous cutoff temperature was twice lower [14].

### C. Hall effect and magnetoresistance

The results of Hall effect measurements are shown in Fig. 2(a). Positive Hall resistivity in positive magnetic field confirms hole-type conductivity, reported in Ref. [7]. However,  $\rho_{xy}(B)$  is not linear in the whole range of magnetic field. At  $T = 2$  K, a very weak change of its slope occurs around magnetic field of 1 T, with temperature increasing this characteristic magnetic field also grows to 4.5 and 6 T, at 100 and 300 K, respectively. Such behavior indicates multiband electronic structure in YPtBi. We tried to fit the two-band

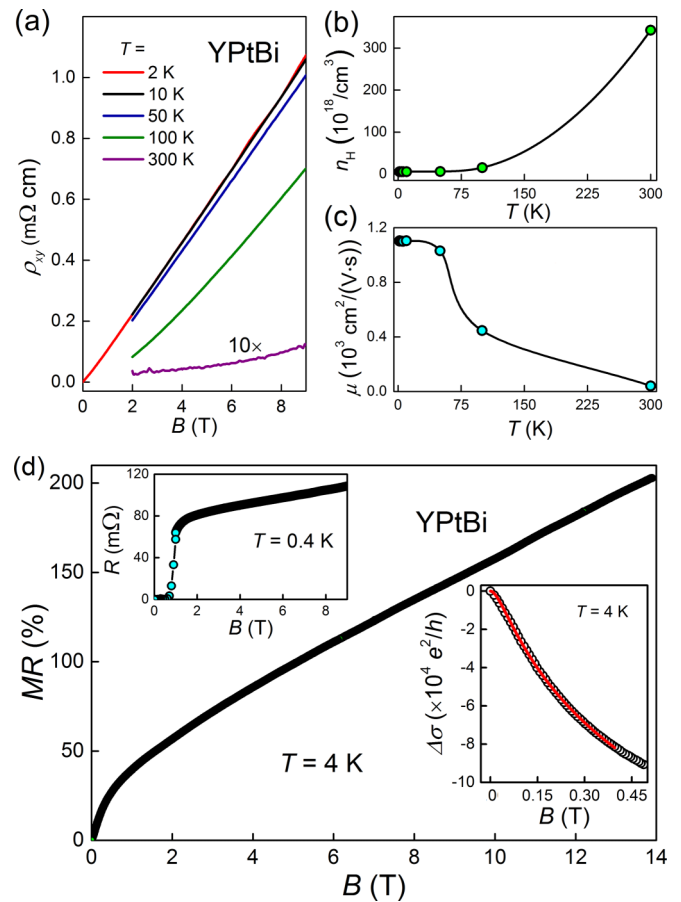


FIG. 2. (a) Hall resistivity of single-crystalline YPtBi as a function of magnetic field measured at several temperatures in the range 2–300 K. In fields stronger than 5 T and temperatures below 10 K clear oscillations of  $\rho_{xy}$  appear. (b),(c) Temperature dependence of the carrier concentration and the Hall mobility, respectively. Solid lines are guides for the eye. (d) Magnetoresistance of YPtBi as a function of magnetic field, measured at  $T = 4$  K. Lower inset: sheet conductance of YPtBi at  $T = 4$  K versus magnetic field. The red solid line represents the fit to the Hikami-Larkin-Nagaoka model (see the text). Upper inset: magnetic field dependence of the resistance of YPtBi taken at  $T = 0.4$  K.

model to our data, but attempts were futile, since the fits yielded parameters, which were very strongly dependent on each other. Most likely it was due to relatively small difference in mobilities of holes and electrons, which also brought almost linear behavior of  $\rho_{xy}(B)$ . Thus we used the single-carrier Drude model and from values of  $\rho_{xy}$  taken at magnetic field 9 T calculated carrier concentrations,  $n_H$ , and mobilities,  $\mu$ , for YPtBi. We keep in mind that obtained in such way values of  $n_H$  should be interpreted with caution and provide only lower limit of actual concentration, due to the multiband character of the compound.

The temperature dependence of  $n_H$  in YPtBi is shown in Fig. 2(b). In the temperature range from 2 to 50 K,  $n_H$  hardly changes and equals  $\approx 5.6 \times 10^{18} \text{ cm}^{-3}$ . Above 50 K, the carrier concentration begins to increase, and attains  $3.4 \times 10^{20} \text{ cm}^{-3}$  at room temperature. This behavior of  $n_H(T)$  resembles that described by Butch *et al.* with a difference in the magnitudes, as they estimated  $n_H = 2 \times 10^{18} \text{ cm}^{-3}$  at 2 K and a tenfold increased value at 300 K [7]. On the other hand, Ref. [30] reported  $n_H = 6.8 \times 10^{18} \text{ cm}^{-3}$  at low temperatures, which only tripled at 300 K. Such big differences in values of  $n_H$  seem to be caused by sample- and temperature-dependent contributions of different bands in total conductivity.

Remarkably, the carrier concentration in YPtBi at low temperatures is at least three orders of magnitude smaller than its theoretically estimated lower limit necessary for conventional pairing superconductivity in this compound [16]. This finding is in line with the odd-parity character of the superconducting state in YPtBi, suggested by Bay *et al.* [8]. Figure 2(c) displays the temperature variation of the Hall mobility,  $\mu$ , in YPtBi. The value observed at 300 K is  $\mu = 40 \text{ cm}^2 \text{ V}^{-1} \text{ s}^{-1}$ , whilst those below 50 K are  $\approx 1100 \text{ cm}^2 \text{ V}^{-1} \text{ s}^{-1}$ .

It is interesting to compare our results to Hall concentration and mobility very recently reported for the heavy-lanthanides-bearing *RPtBi* series ( $R = \text{Gd, Dy, Tm, and Lu}$ ) and plotted against the lattice parameter [31]. At 300 K our values  $n_H = 3.4 \times 10^{20} \text{ cm}^{-3}$  and  $\mu = 40 \text{ cm}^2 \text{ V}^{-1} \text{ s}^{-1}$ , place YPtBi properly between GdPtBi ( $n_H = 5.5 \times 10^{19} \text{ cm}^{-3}$ ,  $\mu \sim 260 \text{ cm}^2 \text{ V}^{-1} \text{ s}^{-1}$ ) and TmPtBi ( $n_H \sim 10^{21} \text{ cm}^{-3}$ ,  $\mu \sim 3 \text{ cm}^2 \text{ V}^{-1} \text{ s}^{-1}$ ), which corroborates the conclusion of Ref. [31] that “the trend along the series is steric rather than magnetic in origin”. Values of Hall coefficient we measured at 300 K,  $\rho_{xy}/B \sim 0.1 \text{ n}\Omega \text{ cm/Oe}$ , resemble most closely those of TmPtBi (cf. Fig. 9c of Ref. [31]).

Figure 2(d) depicts the results of magnetoresistance (*MR*) measurements of YPtBi at temperatures 0.4 K and 4 K, in magnetic fields up to 9 T and 14 T, respectively. At  $T = 0.4 \text{ K}$  a behavior typical for a superconducting material is observed [see the upper inset to Fig. 2(d)]. At 4 K *MR* first rapidly increases with increasing field, showing a concave curvature, but then it becomes nearly linear up to the strongest fields achievable [cf. the main panel of Fig. 2(d)]. *MR* reaches 205% in 14 T, which is a quite large value, very close to that which we could estimate from Fig. 2 of Butch *et al.* [7].

The shape of *MR(B)* in weak magnetic fields has already been considered for YPtBi in terms of the weak antilocalization (WAL) effect [7,30], evidenced also in several TIs [14,32,33]. Following that approach we fitted magneto-

conductance with the Hikami-Larkin-Nagaoka [34] function,  $\frac{\eta e^2}{2\pi^2 \hbar} [\psi(\frac{1}{2} + \frac{\hbar}{4eL_\phi^2 B}) - \ln(\frac{\hbar}{4eL_\phi^2 B})]$ , where  $\eta$  is a prefactor depending on the strength of spin-orbit coupling and on the type of localization,  $L_\phi$  is a phase coherence length, and  $\psi(x)$  is a digamma function. The fit, depicted in the lower inset to Fig. 2(d), was of good quality and yielded  $L_\phi = 97 \text{ nm}$  and  $\eta = -1.9 \times 10^5$ . Comparable values of  $L_\phi$  and  $\eta$  were found previously for YPtBi, LuPdBi, and HoPdBi [7,14,15,30]. Similar magnitudes of the prefactor  $\eta$ , several orders larger than expected for purely 2D TI states, were already reported for YPtBi, LuPtBi, LuPdBi, and LuPtSb [7,12,30,35] and rationalized by assuming bulk or sidewall channels of electron transport [36].

#### D. Shubnikov–de Haas oscillations

In addition to WAL and nonsaturating linear *MR*, we observed for our single crystals of YPtBi another fingerprint of possible TI states, namely Shubnikov–de Haas (SdH) oscillations. At temperatures up to 10 K, both the electrical resistivity and the Hall resistivity were found to oscillate in high magnetic fields. Quantum oscillations of the resistivity of single-crystalline YPtBi have already been observed by Butch *et al.*, who determined the effective cyclotron mass,  $m^* = 0.15m_e$  ( $m_e$  is the free electron mass), the oscillation frequency 46 T and estimated, within spherical FS approximation, the carrier concentration of  $1.7 \times 10^{18} \text{ cm}^{-3}$  (cf. Ref. [7]). Interestingly, they have noticed also a node at  $0.12 \text{ T}^{-1}$ , due to beating, and attributed this effect to spin-orbit splitting of the Fermi surface and shifts in phase of the oscillations.

Figure 3(a) represents the SdH oscillations of the Hall resistivity of YPtBi, visualized upon subtracting from the measured data a linear component [cf. Fig. 2(a)]. No sign of FS splitting is seen. The temperature dependence of the Hall resistivity oscillations amplitude can be expressed as  $\Delta\rho_{xy} \propto \lambda(T)/\sinh(\lambda(T))$ , where  $\lambda(T) = 2\pi^2 k_B T m^*/(\hbar e B)$  [37]. Fitting this equation to the experimental data of YPtBi [see Fig. 3(b)] yielded  $m^* = 0.22m_e$ , which is only slightly larger than the value reported before [7].

The oscillating component  $\Delta\rho_{xy}$  was analyzed [see the upper inset to Fig. 3(a)] in terms of the standard Lifshitz-Kosevich (LK) expression:

$$\Delta\rho_{xy} \propto \exp^{-\lambda_D} \lambda_T \sqrt{1/B} \cos(2\pi(F/B + \beta + 1/2)), \quad (1)$$

where  $\lambda_D = 2\pi^2 k_B T_D m^*/(\hbar e B)$ ,  $F$  stands for the oscillation frequency,  $T_D$  is the Dingle temperature,  $\beta$  is the phase shift that directly corresponds to the Berry phase, and  $\lambda_T = \lambda(T)/\sinh(\lambda(T))$  [37]. With  $m^*$  fixed at  $0.22m_e$  the LK formula was fit to the experimental data of YPtBi, which yielded  $T_D = 5.1(2) \text{ K}$ ,  $F = 24.7(1) \text{ T}$ ,  $\beta = 0.35(1)$ , and the Berry phase  $0.7\pi$  at 1.85 K. The oscillation frequency was found temperature independent. Another way in which the Dingle temperature could be obtained is the so-called Dingle analysis, depicted in the inset to Fig. 3(b). The value of  $T_D$  derived from the slope of the linear fit amounts to 6.45 K, being thus fairly similar to that obtained from the LK function fitting. Knowing  $T_D$  allows estimating the surface scattering time  $\tau_s = \hbar/(2\pi k_B T_D) = 1.88 \times 10^{-13} \text{ s}$ . It is worth noting that the transport scattering time evaluated from the

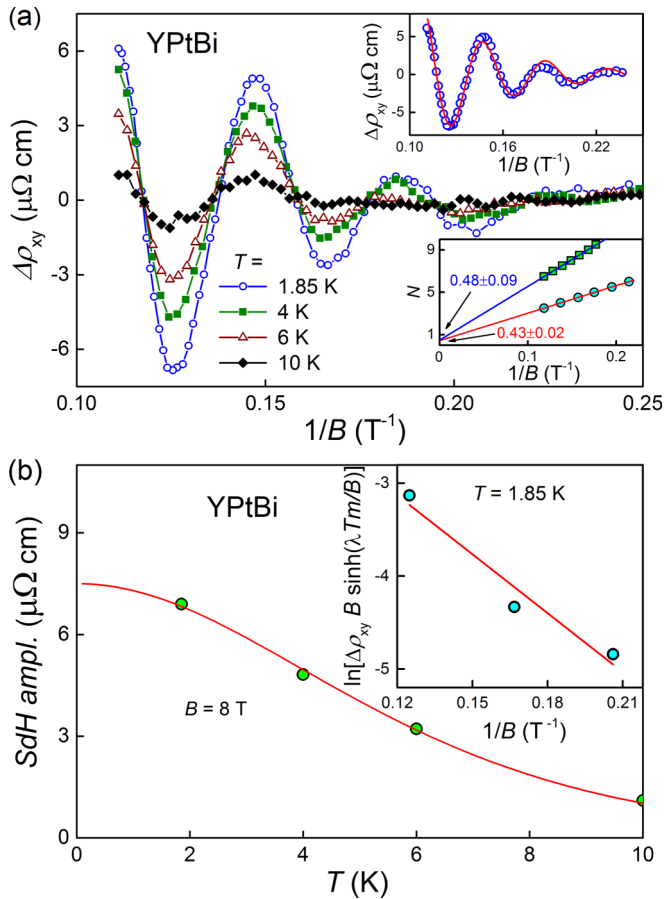


FIG. 3. (a) Shubnikov-de Haas (SdH) oscillations of  $\rho_{xy}$  measured at 1.85, 4, 6, and 10 K. Upper inset: SdH oscillations at  $T = 1.85$  K. The solid line represents the LK fit discussed in the text [Eq. (1)]. Lower inset: Landau-level index plot. The solid straight lines fitted to the LL data (circles for  $\rho_{xy}$ , squares for  $\rho_{xx}$ ) have the intercepts indicated by arrows. (b) Temperature dependence of the SdH amplitude observed in a magnetic field of 8 T. The solid line is the LK fit (see the text). Inset: Dingle plot for the oscillations measured at 1.85 K. Solid line represents linear fit determining the Dingle temperature (see the text).

Hall carrier concentration  $\tau_t = m^*/(e^2 n_H \rho) = 1.58 \times 10^{-13}$  s is nearly identical to  $\tau_s$ . The value of the scattering time derived for our single crystals is almost twice larger than that reported by Butch *et al.* [7]. Assuming circular cross section of the Fermi surface one obtains from the Onsager's relation [37], the Fermi wave vector  $k_F^{\text{SdH}} = \sqrt{2\pi eF/\hbar} = 2.74 \times 10^6 \text{ cm}^{-1}$ , which corresponds to the 2D carrier density  $n_{2D} = 6 \times 10^{11} \text{ cm}^{-2}$ . Other parameters which can be derived are the Fermi velocity  $v_F = \hbar k_F^{\text{SdH}}/m^* \approx 1.4 \times 10^5 \text{ ms}^{-1}$ , the Fermi energy  $E_F = m^* v_F^2/2 \approx 12.8 \text{ meV}$ , the mean-free path  $l_{\text{SdH}} = v_F \tau_s = 26.8 \text{ nm}$ , and the carrier mobility  $\mu_s = e\tau_s/m^* = el/\hbar k_F^{\text{SdH}} = 1486 \text{ cm}^2 \text{ V}^{-1} \text{ s}^{-1}$ . Comparison of the parameters obtained from the SdH oscillations analysis, especially  $\tau_s$  and  $\mu_s$ , and those derived from the Hall data at the lowest temperatures, especially  $\tau_t$  and  $\mu$ , shows their very good agreement.

We examined also angular dependence of  $\rho_{xy}(B^{-1})$  oscillations. When the field was tilted from [111] towards [001] direction by an angle  $\theta$  the SdH frequency increased as

$\approx 1/\cos\theta$ . At  $\theta \approx 55^\circ$  (i.e., the field along [001])  $F$  reached maximum value of 42 T and started to decrease upon further rotation. This maximum value is very close to 46 T reported by Butch *et al.* [7]. In turn, our analysis of the SdH oscillations in the transverse MR in field applied along [001] [see Fig. 2(d)] yielded  $F = 49$  T. The observed angle dependence of the SdH frequency may be explained assuming the presence of strongly elongated electron FS pockets of cigarlike shape located between  $\Gamma$  and  $L$  points of Brillouin zone, with their axes along  $\langle 111 \rangle$  directions. The cross section of such FS pocket changes as  $\approx 1/\cos\theta$  when the field is tilted from its axis by  $\theta$  [38], but when the field passes the [001] direction the SdH signal from another pocket of the same type takes over and  $F$  starts decreasing.

Our experimental findings are consistent with the electronic structure calculations performed by Meinert [16], while contradicting those reported in Refs. [5,6]. Nevertheless, Meinert's results also show band inversion and do not exclude topologically nontrivial states. Thus we may hypothesize that at low temperatures the electrical current flows in single-crystalline YPtBi almost only due to metallic surface states and the bulk of material is nearly completely insulating. The observation of two-channel conductivity in YPtBi [see Fig. 1(c)] strengthens this conjecture, and expands its validity to higher temperatures, at least up to 40 K.

Strong support for the nontrivial topology of YPtBi band structure, arising directly from the analysis of the SdH oscillations, is nonzero Berry phase. The Berry phase can be also determined employing a Landau level (LL) index analysis. First, following the discussion on proper construction of the LL index plot [29], the Hall conductance  $G_{xy} = R_{xy}/(R_{xy}^2 + R_{xx}^2)$  at  $T = 1.85$  K was derived. Next, positions of the extrema in  $G_{xy}(1/B)$  were identified by differentiating this function. The maxima in  $dG_{xy}/d(1/B)$  were labeled by integer numbers, while the minima by half-integer numbers, appropriately for a system with dominant hole-charge carriers [39]. As can be inferred from the lower inset to Fig. 3(a), a linear fit to the LL index data yielded an intercept of 0.43, which corresponds to the  $0.86\pi$  Berry phase. Though there is a little difference between the latter value and  $0.7\pi$  obtained from the LK analysis, both are nontrivial being much closer to the theoretical value of  $\pi$  characteristic of Dirac fermions than to zero expected for Schrödinger fermions. Slightly reduced Berry phase with respect to the theoretical one may arise due to Zeeman coupling and/or small deviation from the ideal linear dispersion of Dirac fermions [40]. Analysis of weaker SdH oscillations of  $\rho_{xx}$  at 0.4 K [upper inset of Fig. 2(d)] also resulted in nontrivial Berry phase of  $0.96\pi$  [cf. lower inset to Fig. 3(a)].

### E. Heat capacity

Figure 4 shows the low-temperature dependence of specific heat capacity,  $C$ , measured in zero magnetic field. Our results at higher temperatures are fairly close to those published in literature: at 20 K we measured 6 J/mol K, while Ref. [41] reported 6.6 J/mol K (at 10 K: 1 J/mol K and 0.9 J/mol K, respectively). At lower temperatures we observed discrepancies with Ref. [41], indicating again that the electronic structure of YPtBi is strongly sample dependent.

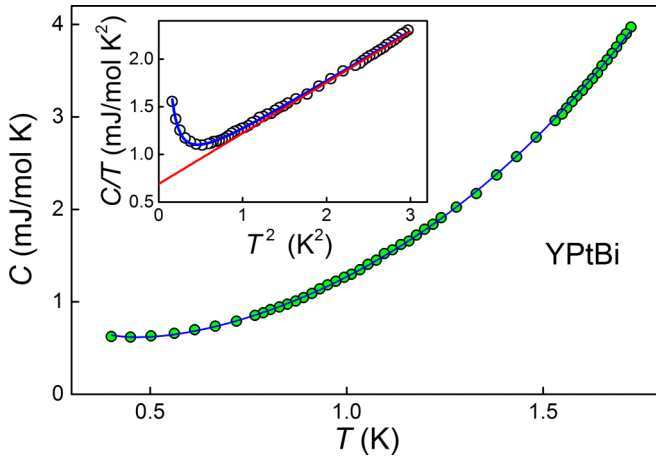


FIG. 4. Low temperature dependent specific heat capacity of YPtBi. Blue solid line represents the results of fitting with Eq. (2). Inset: specific heat capacity over temperature versus squared temperature. Blue solid line corresponds to the fit described by equation  $C/T = \gamma + \beta T^2 + \delta T^{-3}$ . Red solid line represents the same function redrawn without nuclear Schottky term  $\delta T^{-3}$ , showing the intercept  $\gamma = 0.69$  mJ/mol K<sup>2</sup>.

Observed behavior of  $C(T)$  cannot be described by standard model for nonmagnetic metal. As emphasized in the inset of Fig. 4,  $C/T$  shows a distinct increase of  $C/T$  below 0.8 K. This effect can be attributed to nuclear contribution. Here both bismuth and yttrium can be responsible for this effect in YPtBi, due to rather big values of nuclear quadrupole moment. Contribution of the nuclear Schottky effect may be approximated as [42]  $C_{\text{Sch}} \propto T^{-2}$ . We thus fitted our experimental data with equation

$$C(T) = \gamma T + \beta T^3 + \delta T^{-2}, \quad (2)$$

where  $\gamma$  is the Sommerfeld electronic heat capacity coefficient and  $\beta$  is Debye lattice heat capacity coefficient. The fit is represented by the solid blue lines in Fig. 4. Analyzing the experimental data in terms of this formula we evaluated the following parameters:  $\gamma = 0.69$  mJ/mol K<sup>2</sup>,  $\beta = 0.53$  mJ/mol K<sup>4</sup>, and  $\delta = 0.052$  mJ K/mol.

From the value of  $\beta$  one finds the Debye temperature,  $\Theta_D = (36R_g\pi^4/5\beta)^{1/3} = 222$  K, where  $R_g$  is the gas constant. We note that the our  $\gamma$  is much bigger than 0.1 mJ/mol K<sup>2</sup> reported by Pagliuso *et al.* [41] but they analyzed data collected at a significantly higher temperature range: 1.5–3.5 K. When we analyzed our data in the same temperature interval we got  $\gamma = 0.4$  mJ/mol K<sup>2</sup>, which is still bigger than that obtained in Ref. [41].

Similar to LuPtBi, LuPdBi, and several antiferromagnetically ordered, superconducting half-Heusler phases, including HoPdBi (Refs. [14,15,43,44]), no anomaly in specific heat capacity is visible at the superconducting phase transition. Moreover, knowing the values of effective mass and Fermi wave vector derived from SdH oscillations and assuming that YPtBi

has 3D spherical Fermi surface we calculated the Sommerfeld coefficient:  $\gamma = k_B^2 V m^* k_F / 3\hbar^2 = 0.014$  mJ/mol K<sup>2</sup>, a value nearly 50 times smaller than that derived from  $C(T)$  analysis.

#### IV. CONCLUSIONS

We confirmed the superconductivity of YPtBi single crystals with characteristic values of  $T_c = 0.97$  K and  $B_{c2} \approx 1.6$  T, being fairly similar to previously reported [7–9]. Lack of anomaly near the onset of superconductivity on the temperature dependence of specific heat capacity is remarkable, because it might reflect the superconductivity of surface states which occupy only the small fraction of the whole sample volume.

Magnetoresistance of YPtBi has several features typical for topologically nontrivial materials: (i) at low magnetic fields a sharp increase consistent with WAL effect, (ii) linear and nonsaturating behavior in high magnetic fields and wide range of temperatures, and (iii) quantum oscillations in magnetic field.

The analysis of SdH oscillations brought us some insight into the Dirac fermion nature of carriers in YPtBi. Small value of effective mass and nonzero Berry phase are common features of Dirac systems with linear energy dispersion. We determined the Berry phase in two different ways, from the fitting Lifshitz-Kosevich formula to experimental data and with the help of Landau index plot—in both cases Berry phase is nonzero and very close to theoretical  $\pi$  value for Dirac fermion.

Comparison of Sommerfeld coefficients derived from specific heat and quantum oscillation results suggests that SdH oscillations come from the electrons that occupy the Fermi surface much smaller than the one which brings out the observed specific heat capacity. Thus SdH oscillations seem to originate from a 2D Fermi surface (formed by Dirac fermions) or from small pockets of 3D Fermi surface (like those elongated electron pockets predicted by Meinert's calculations [16]). These two possible sources of SdH oscillations do not exclude each other. Dirac cone always forms around inverted 3D bands, and when topological gap is below or above the Fermi level, a cross section of that Dirac cone consisting of 2D surface states envelops closely a pocket of 3D Fermi surface. Frequencies and angular dependence of SdH oscillations corresponding to these 2D and 3D states may be very similar, making it difficult to distinguish 2D surface states from anisotropic 3D pockets. This obstacle seems to be present also in the case of YPtBi; however, the Berry phase points strongly in favor of Dirac states.

Our results on electronic properties revealed several characteristics of nontrivial topology nature in YPtBi single crystals. But the final confirmation of such unusual properties must be sought via additional spectroscopic investigation. A report on photoemission study of YPtBi has been posted [45].

#### ACKNOWLEDGMENT

This work was supported by the National Science Centre of Poland, Grant No. 2015/18/A/ST3/00057.

[1] T. Graf, C. Felser, and S. S. P. Parkin, *Prog. Solid State Chem.* **39**, 1 (2011).

[2] F. Casper, T. Graf, S. Chadov, B. Balke, and C. Felser, *Semicond. Sci. Technol.* **27**, 063001 (2012).

- [3] S. Chadov, X. Qi, J. Kübler, G. H. Fecher, C. Felser, and S. C. Zhang, *Nat. Mater.* **9**, 541 (2010).
- [4] H. Lin, L. A. Wray, Y. Xia, S. Xu, S. Jia, R. J. Cava, A. Bansil, and M. Z. Hasan, *Nat. Mater.* **9**, 546 (2010).
- [5] W. Al-Sawai, H. Lin, R. S. Markiewicz, L. A. Wray, Y. Xia, S.-Y. Xu, M. Z. Hasan, and A. Bansil, *Phys. Rev. B* **82**, 125208 (2010).
- [6] W. Feng, D. Xiao, Y. Zhang, and Y. Yao, *Phys. Rev. B* **82**, 235121 (2010).
- [7] N. P. Butch, P. Syers, K. Kirshenbaum, A. P. Hope, and J. Paglione, *Phys. Rev. B* **84**, 220504 (2011).
- [8] T. V. Bay, T. Naka, Y. K. Huang, and A. de Visser, *Phys. Rev. B* **86**, 064515 (2012).
- [9] T. V. Bay, M. Jackson, C. Paulsen, C. Baines, A. Amato, T. Orvis, M. Aronson, Y. Huang, and A. de Visser, *Solid State Commun.* **183**, 13 (2014).
- [10] F. F. Tafti, T. Fujii, A. Juneau-Fecteau, S. René de Cotret, N. Doiron-Leyraud, A. Asamitsu, and L. Taillefer, *Phys. Rev. B* **87**, 184504 (2013).
- [11] Y. Pan, A. M. Nikitin, T. V. Bay, Y. K. Huang, C. Paulsen, B. H. Yan, and A. de Visser, *Europhys. Lett.* **104**, 27001 (2013).
- [12] G. Xu, W. Wang, X. Zhang, Y. Du, E. Liu, S. Wang, G. Wu, Z. Liu, and X. X. Zhang, *Sci. Rep.* **4**, 5709 (2014).
- [13] G. Goll, M. Marz, A. Hamann, T. Tomanic, K. Grube, T. Yoshino, and T. Takabatake, *Physica B* **403**, 1065 (2008).
- [14] O. Pavlosiuk, D. Kaczorowski, and P. Wiśniewski, *Sci. Rep.* **5**, 9158 (2015).
- [15] O. Pavlosiuk, D. Kaczorowski, X. Fabreges, A. Gukasov, and P. Wiśniewski, *Sci. Rep.* **6**, 18797 (2016).
- [16] M. Meinert, *Phys. Rev. Lett.* **116**, 137001 (2016).
- [17] L. Fu and C. L. Kane, *Phys. Rev. Lett.* **100**, 096407 (2008).
- [18] C. Nayak, S. H. Simon, A. Stern, M. Freedman, and S. Das Sarma, *Rev. Mod. Phys.* **80**, 1083 (2008).
- [19] Y. S. Hor, A. J. Williams, J. G. Checkelsky, P. Roushan, J. Seo, Q. Xu, H. W. Zandbergen, A. Yazdani, N. P. Ong, and R. J. Cava, *Phys. Rev. Lett.* **104**, 057001 (2010).
- [20] L. Fu and E. Berg, *Phys. Rev. Lett.* **105**, 097001 (2010).
- [21] S. Sasaki, M. Kriener, K. Segawa, K. Yada, Y. Tanaka, M. Sato, and Y. Ando, *Phys. Rev. Lett.* **107**, 217001 (2011).
- [22] R. D. Zhong, J. A. Schneeloch, T. S. Liu, F. E. Camino, J. M. Tranquada, and G. D. Gu, *Phys. Rev. B* **90**, 020505 (2014).
- [23] L. P. He, Z. Zhang, J. Pan, X. C. Hong, S. Y. Zhou, and S. Y. Li, *Phys. Rev. B* **88**, 014523 (2013).
- [24] L. Fang, C. C. Stoumpos, Y. Jia, A. Glatz, D. Y. Chung, H. Claus, U. Welp, W.-K. Kwok, and M. G. Kanatzidis, *Phys. Rev. B* **90**, 020504 (2014).
- [25] S. Sasaki, K. Segawa, and Y. Ando, *Phys. Rev. B* **90**, 220504 (2014).
- [26] B. Nowak and D. Kaczorowski, *J. Phys. Chem. C* **118**, 18021 (2014).
- [27] C. Liu, Y. Lee, T. Kondo, E. D. Mun, M. Caudle, B. N. Harmon, S. L. Budko, P. C. Canfield, and A. Kaminski, *Phys. Rev. B* **83**, 205133 (2011).
- [28] B. Nowak, O. Pavlosiuk, and D. Kaczorowski, *J. Phys. Chem. C* **119**, 2770 (2015).
- [29] Y. Ando, *J. Phys. Soc. Jpn.* **82**, 102001 (2013).
- [30] C. Shekhar, E. Kampert, T. Förster, A. K. Nayak, M. Nicklas, and C. Felser, [arXiv:1502.00604](https://arxiv.org/abs/1502.00604).
- [31] E. Mun, S. L. Bud'ko, and P. C. Canfield, *Phys. Rev. B* **93**, 115134 (2016).
- [32] M. Liu, J. Zhang, C.-Z. Chang, Z. Zhang, X. Feng, K. Li, K. He, L.-l. Wang, X. Chen, X. Dai, Z. Fang, Q.-K. Xue, X. Ma, and Y. Wang, *Phys. Rev. Lett.* **108**, 036805 (2012).
- [33] S. X. Zhang, R. D. McDonald, A. Shekhter, Z. X. Bi, Y. Li, Q. X. Jia, and S. T. Picraux, *Appl. Phys. Lett.* **101**, 202403 (2012).
- [34] S. Hikami, A. I. Larkin, and Y. Nagaoka, *Prog. Theor. Phys.* **63**, 707 (1980).
- [35] D. Hou, G. Su, Y. Tian, X. Jin, S. A. Yang, and Q. Niu, *Phys. Rev. Lett.* **114**, 217203 (2015).
- [36] V. E. Sacksteder, K. B. Arnardottir, S. Kettemann, and I. A. Shelykh, *Phys. Rev. B* **90**, 235148 (2014).
- [37] D. Shoenberg, *Magnetic Oscillations in Metals* (Cambridge University Press, Cambridge, UK, 1984).
- [38] When FS pocket is well approximated by an ellipsoid, its cross section changes as  $S \propto (r^{-2} \sin^2 \theta + \cos^2 \theta)^{-1/2}$  [this holds exactly for a two-axial ellipsoid described by  $(x/A)^2 + (y/B)^2 + (z/C)^2 = 1$  and  $r = B/A$ ]. For small  $\theta$  and  $r \gg 1$  this function is very close to  $1/\cos \theta$ .
- [39] A. A. Taskin, F. Yang, S. Sasaki, K. Segawa, and Y. Ando, *Phys. Rev. B* **89**, 121302 (2014).
- [40] A. A. Taskin and Y. Ando, *Phys. Rev. B* **84**, 035301 (2011).
- [41] P. G. Pagliuso, C. Rettori, M. E. Torelli, G. B. Martins, Z. Fisk, J. L. Sarrao, M. F. Hundley, and S. B. Oseroff, *Phys. Rev. B* **60**, 4176 (1999).
- [42] E. S. R. Gopal, *Specific Heats at Low Temperatures* (Springer US, Boston, MA, 1966).
- [43] E. D. Mun, S. L. Bud'ko, C. Martin, H. Kim, M. A. Tanatar, J.-H. Park, T. Murphy, G. M. Schmiedeshoff, N. Dilley, R. Prozorov, and P. C. Canfield, *Phys. Rev. B* **87**, 075120 (2013).
- [44] Y. Nakajima, R. Hu, K. Kirshenbaum, A. Hughes, P. Syers, X. Wang, K. Wang, R. Wang, S. R. Saha, D. Pratt, J. W. Lynn, and J. Paglione, *Sci. Adv.* **1**, e1500242 (2015).
- [45] Z. Liu *et al.*, [arXiv:1602.05633](https://arxiv.org/abs/1602.05633).